LA-UR 98-3076

Multiple concentric annuli for characterizing spatially nonuniform backgrounds

James Theiler and Jeff Bloch
Space and Remote Sensing Sciences Group, NIS-2, MS-D436,
Los Alamos National Laboratory, Los Alamos, NM 87545

ABSTRACT

A method is presented for estimating the background at a given location on a sky map by interpolating the estimated background from a set of concentric annuli which surround this location. If the background is nonuniform but smoothly varying, this method provides a more accurate (though less precise) estimate than can be obtained with a single annulus. Several applications of multi-annulus background estimation are discussed, including direct testing for point sources in the presence of a nonuniform background, the generation of "surrogate maps" for characterizing false alarm rates, and precise testing of the null hypothesis that the background is uniform.

Subject headings: methods: data analysis — methods: statistical — surveys — stars: imaging — ultraviolet: stars

1. Introduction

This study is motivated by the search for rare bright transient point sources in count-limited sky maps generated from data taken by the ALEXIS (Array of Low Energy X-ray Imaging Sensors) satellite. Each of the six telescopes in the array uses a spherical narrow-band normal-incidence multi-layer mirror with a micro-channel plate detector at the prime focus to detect individual EUV photons over a wide 33^o field (Priedhorsky et al. 1988; Bloch et al. 1993). The data are taken in a scanning survey mode, with almost half of the sky (the anti-solar hemisphere) covered every fifty seconds. Individual photons are time-tagged, and after accounting for spacecraft attitude as a function of time (Psiaki et al. 1997), each photon is identified with a position on the sky. In this original form, the "map" is a photon event list, but in practice, these photons are binned into square pixels in a Hammer-Aitoff or a quadrilateralized spherical cube projection (Greisen & Calabretta 1995; Greisen & Calabretta 1996) of the sky. For a given candidate point source location, we estimate a source strength by counting photons in a small region of the map about the size of the telescope point spread function (more accurate estimates can be obtained by convolving the photon counts with the point spread function), and comparing that to an estimate of the background.

If quantitative models are available for all of the various noise sources in the detector and on the sky, then *ab initio* estimates of the background can be made. To be useful, these models must be accurate and reliable, and this is not always possible; for ALEXIS, one of the main reasons for going into space was to identify and quantify these various backgrounds for this new multi-layer instrument technology. A simple alternative is to estimate the background by looking at count rates in the vicinity of the candidate point source (*e.g.,* see Bowyer et al. 1996). Annular regions are particularly useful, since they are insensitive to linear gradients in the background, but there is still an implicit assumption that the background is spatially uniform (or at worst has only linear variation) over the area that includes the point source location and the background estimation region.

With the ALEXIS data, the spatial nonuniformity of the background is quite evident (see figure 1a), and arises from a number of effects: among these are uneven exposure of the scanning telescopes, telescope vignetting, pinhole leaks, detector masks, time-varying high energy penetrating particle flux, an anomalous background component which varies with the angle between the look direction and the spacecraft velocity vector (Bloch et al. 1994), motion of the moon across the field, and possibly even the spatial structure inherent in the diffuse X-ray sky. In this study, we are not concerned with nonuniformities arising from source confusion since point sources are relatively sparse at the ALEXIS sensitivity. Most of these effects are approximately known, and work is in progress to more accurately model them. However, our approach for point source detection is to estimate background from the count map itself.

In this article, we will describe the use of multiple concentric annuli for characterizing a spatially nonuniform background. The most direct application is the estimation of background at a candidate point source location. The multiple-annulus approach is mathematically equivalent to fitting the background with a two-dimensional polynomial of order $q = 2n-1$, where n is the number of annuli. Direct fits, even for relatively low order q, can be unwieldy, but by integrating these polynomials over concentric annuli, we find that the interpolation procedure can be considerably simplified. With two annuli, for example, we effectively fit a cubic polynomial, but we compute only two coefficients instead of ten.

If multiple-annulus estimates of the background can be made more accurate, then a point source detection algorithm that is based on these better estimates will be more sensitive to real point sources for a fixed rate of false alarms. A low false alarm rate is always desirable, but what is particularly important is that the false alarm rate be well calibrated. We show how this can be done using multiple-annulus methods to estimate a smooth but nonuniform estimate of the background. From this background, one then generates a Monte-Carlo ensemble of "surrogate" maps, and by applying the point source detection algorithm to these maps (which have no point sources), one can estimate the false alarm rate. Finally, we will show how multiple annuli can also be used to characterize the magnitude of the background nonuniformity. In particular, we will describe a test of the null hypothesis that the background is uniform. The test, based on counts in concentric annuli, is especially sensitive to the nonuniformities that lead to poor estimates of the background level at the center of the annuli, yet is completely insensitive to linear gradients which have no effect on background estimates at the center of the annuli.

In Section 2, we will introduce notation, and then derive the linear combination of background annuli counts that provides an unbiased estimator for background in a source region. We will consider in particular the use of two annuli, the simplest and probably most useful case, as well as the limit of an infinite number of annuli. In Section 3, we will derive the bias and variance (a.k.a. accuracy and precision) of multiple annulus estimators, compare the performance of single and multiple annulus methods, derive optimal annulus partitions, and suggest heuristic algorithms which trade off bias and variance error. In Section 4, we will illustrate the use of multiple annuli on two example data sets, one real and one artificial. In that section, we will provide four different applications of multiple annuli estimators: estimating background level, detecting point sources, generating surrogate maps, and quantifying background nonuniformity.

2. Background estimation with multiple annuli

In this section, we will derive expressions for the average background in a source region as a linear function of the backgrounds integrated over annular regions surrounding the source. We will derive separate expressions for square and circular regions, but both will have the property that the coefficients of the linear combination depend only on the geometry of the annuli.

For a given region $\mathcal{S}$ of a sky map, we will use $N_{\mathcal{S}}$ to denote the observed number of counts (photons) in the region, and $\mathcal{N}_{\mathcal{S}}$ to denote the *expected* number of counts due only to the smoothly varying nonuniform background. These are dimensionless "counts" and should not be confused with the count "rate" (photons per unit time). For a given position (x, y) on the sky map, let $B(x, y)$ denote the "count density" of the background – expected counts per unit area at that position. Then,

$$\mathcal{N}_{\mathcal{S}} = \iint_{\mathcal{S}} B(x, y)\, dx\, dy. \tag{1}$$

The average count density in a region $\mathcal{S}$ is called $B_{\mathcal{S}}$ and is given by

$$B_{\mathcal{S}} = \frac{\mathcal{N}_{\mathcal{S}}}{A_{\mathcal{S}}} = \frac{\iint_{\mathcal{S}} B(x, y)\, dx\, dy}{\iint_{\mathcal{S}} dx\, dy} \tag{2}$$

where $A_{\mathcal{S}}$ is the area of region $\mathcal{S}$.

Here, $\mathcal{N}_{\mathcal{S}}$ is the "true" background level. If there is only background (no point sources) in $\mathcal{S}$, then the actual number of observed counts $N_{\mathcal{S}}$ will be Poisson-distributed with mean $\mathcal{N}_{\mathcal{S}}$. For example, if $\mathcal{S}$ is the annular region around the candidate point source, then we will usually estimate the background level with $\hat{B}_{\mathcal{S}} = \hat{\mathcal{N}}_{\mathcal{S}}/A_{\mathcal{S}} = N_{\mathcal{S}}/A_{\mathcal{S}}$.

In what follows, we will assume that the background count density $B(x, y)$ can be accurately approximated, over a small region around the potential point source, by an order-q Taylor series polynomial[1]:

$$B(x, y) = \sum_{n+m \le q} c_{nm} x^n y^m. \tag{3}$$

The formalism that we will develop applies to both square and circular annuli. Square annuli are more conveniently employed in maps built from square pixels, while circular annuli are more

[1]We recognize that even large order polynomials will not model abrupt discontinuities in the background – these, alas, are all too common in actual practice. Potential point sources near background discontinuities must be treated with special care.

convenient if the data are recorded in a photon event list. We will characterize these annuli in terms of moments, R_k, defined as follows: Let r_i and r_o denote the inner and outer radii of the annulus (a disk is just an annulus with $r_i = 0$). It will turn out that only the even moments are important, so we will *define*

$$R_k(r_i, r_o) \equiv \frac{1}{k+1} \frac{r_o^{2k+2} - r_i^{2k+2}}{r_o^2 - r_i^2} \quad (4)$$

$$= \frac{1}{k+1} \sum_{j=0}^{k} r_o^{2j} r_i^{2k-2j}. \quad (5)$$

For circular annuli, this corresponds precisely to the $2k$-th moment $\langle r^{2k} \rangle$. For square annuli, there is a k-dependent prefactor which is not important for our purposes.

2.1. Average counts in a square annulus

Let $\mathcal{S}$ be a square of side $2r$ (*i.e.*, of "radius" r). Then, from equation (1) and equation (3), we can write the expected number of counts in the square as

$$\mathcal{N}_{\mathcal{S}} = \sum_{n+m \leq q} c_{nm} \int_{-r}^{r} x^n \, dx \int_{-r}^{r} y^m \, dy. \quad (6)$$

Since the square is symmetric in both x and y, it follows that $\int_{-r}^{r} dx \, x^n \int_{-r}^{r} dy \, y^m$ is zero unless both n and m are even. So we need only perform the sum over even indices; that is:

$$\mathcal{N}_{\mathcal{S}} = \sum_{2n+2m \leq q} c_{2n,2m} \int_{-r}^{r} x^{2n} \, dx \int_{-r}^{r} y^{2m} \, dy \quad (7)$$

$$= \sum_{2n+2m \leq q} c_{2n,2m} \frac{2r^{2n+1}}{2n+1} \frac{2r^{2m+1}}{2m+1} \quad (8)$$

$$= \sum_{2n+2m \leq q} \frac{4c_{2n,2m}}{(2n+1)(2m+1)} r^{2n+2m+2}. \quad (9)$$

For an annulus with inner radius r_i and outer radius r_o, the expected number of counts is given by

$$\mathcal{N}_{\mathcal{S}} = \sum_{2n+2m \leq q} \frac{4c_{2n,2m}}{(2n+1)(2m+1)} \left(r_o^{2n+2m+2} - r_i^{2n+2m+2} \right) \quad (10)$$

Following equation (2), we divide by the area of the annulus to get the count density

$$B_{\mathcal{S}} = \sum_{2n+2m \leq q} \frac{c_{2n,2m}}{(2n+1)(2m+1)} \left(\frac{r_o^{2n+2m+2} - r_i^{2n+2m+2}}{r_o^2 - r_i^2} \right). \quad (11)$$

In particular, if we define

$$L_k = \sum_{j=0}^{k} \frac{k+1}{(2j+1)(2k-2j+1)} c_{2j,2k-2j} \quad (12)$$

and invoke the definition in equation (4), we can write

$$B_{\mathcal{S}} = \sum_{k=0}^{\lfloor q/2 \rfloor} L_k R_k. \tag{13}$$

where L_k depends only on the underlying polynomial, and R_k depends only on the geometry of the annulus. Here $\lfloor q/2 \rfloor$ is the "floor" of $q/2$; that is, the largest integer less than or equal to $q/2$. What is remarkable about this expression is that there are only $1 + \lfloor q/2 \rfloor$ variables (the L_k's) which depend on the $(q+1)(q+2)/2$ polynomial coefficients c_{nm}. If our goal is to estimate $B_{\mathcal{S}}$ for some area $\mathcal{S}$, then we only need to estimate $1 + \lfloor q/2 \rfloor$ separate coefficients.

2.2. Average counts in a circular annulus

It is fairly straightforward to adapt the above derivation to circular annuli. Writing equation (1) in polar coordinates, we get

$$\mathcal{N}_{\mathcal{S}} = \int_{\mathcal{S}} B(x,y)\, dx\, dy = \int_{r_i}^{r_o} r\, dr \int_0^{2\pi} B(r\cos\theta, r\sin\theta)\, d\theta \tag{14}$$

Expanding $B(x,y)$ as a polynomial of degree q we obtain

$$\mathcal{N}_{\mathcal{S}} = \sum_{n+m\le q} c_{nm} \int_{r_i}^{r_o} r\, r^{n+m}\, dr \int_0^{2\pi} \cos^n\theta \sin^m\theta\, d\theta \tag{15}$$

It is clear that $\int_0^{2\pi} \cos^n\theta \sin^m\theta\, d\theta$ vanishes if either n or m are odd (and that it is strictly positive when both n and m are even), so we can rewrite:

$$\mathcal{N}_{\mathcal{S}} = \sum_{2n+2m\le q} c_{2n,2m} \int_0^{r} r\, r^{2n+2m}\, dr \int_0^{2\pi} \cos^{2n}\theta \sin^{2m}\theta\, d\theta \tag{16}$$

Let us define

$$K_{nm} \equiv \frac{1}{2\pi} \int_0^{2\pi} \cos^{2n}\theta \sin^{2m}\theta\, d\theta. \tag{17}$$

One can show that $K_{nm} = (2m-1)!!(2n-1)!!/2^{n+m}(n+m)!$, where $n!! = n(n-2)(n-4)\cdots 1$, but we don't actually need the closed form. In terms of K_{nm}, we can write

$$\mathcal{N}_{\mathcal{S}} = \sum_{2n+2m\le q} \frac{c_{2n,2m}(2\pi K_{nm})}{2n+2m+2} \left(r_o^{2n+2m+2} - r_i^{2n+2m+2} \right) \tag{18}$$

Now, define

$$L_k = \sum_{i=0}^{k} K_{i,k-i}\, c_{2i,2k-2i} \tag{19}$$

so that

$$\mathcal{N}_{\mathcal{S}} = \sum_{k=0}^{\lfloor q/2 \rfloor} \frac{\pi L_k}{k+1} \left(r_o^{2k+2} - r_i^{2k+2} \right) \tag{20}$$

and then combining equation (3) and equation (4)

$$
\begin{aligned}
B_{\mathcal{S}} &= \mathcal{N}_{\mathcal{S}}/\mathrm{area}(\mathcal{S}) && (21)\\
&= \sum_{k=0}^{\lfloor q/2 \rfloor} \frac{\pi L_k}{k+1} \frac{r_o^{2k+2} - r_i^{2k+2}}{\pi r_o^2 - \pi r_i^2} && (22)\\
&= \sum_{k=0}^{\lfloor q/2 \rfloor} L_k R_k. && (23)
\end{aligned}
$$

where, again, the $1 + \lfloor q/2 \rfloor$ variables L_k depend on the underlying polynomial but not on the geometry of the annuli, and the R_k depend only on the annuli.

2.3. Using multiple concentric annuli to estimate source background

The advantage of the decomposition of $B_{\mathcal{S}}$ into a sum of the form given in equation (13), and again in equation (23), can be seen when we try to estimate the background count density in a central region B_{src} from the count densities B_s estimated from each of the concentric annuli.

Assume that the background can be well-modeled (at least in a region containing all the annuli) by an order q polynomial, and that we have $1+\lfloor q/2 \rfloor$ concentric annuli surrounding the point source candidate.

Let R_{ks} denote the R_k value given in equation (4) for the s-th annulus. This is essentially the $2k$-th moment and is a purely geometrical property of the s-th annulus. Let B_s be the average count density in that annulus. Under these assumptions, the $1 + \lfloor q/2 \rfloor$ annuli all satisfy

$$B_s = \sum_{k=0}^{\lfloor q/2 \rfloor} L_k R_{ks} \tag{24}$$

which is a linear system of $1+\lfloor q/2 \rfloor$ equations in $1+\lfloor q/2 \rfloor$ unknowns. In particular, let $\mathcal{R}_{sk}$ denote the s, k element of the inverse of the R_{ks} matrix. That is, $\sum_k \mathcal{R}_{sk} R_{ks'} = \delta_{ss'}$. Then $L_k = \sum_s B_s \mathcal{R}_{sk}$. If the central source region has moments $R_{k,\mathrm{src}}$, then we can write the count density in the central area as

$$B_{\mathrm{src}} = \sum_k L_k R_{k,\mathrm{src}} = \sum_k \sum_s B_s \mathcal{R}_{sk} R_{k,\mathrm{src}} \tag{25}$$

or, if we define

$$\beta_s \equiv \sum_k \mathcal{R}_{sk} R_{k,\mathrm{src}}, \tag{26}$$

then

$$B_{\mathrm{src}} = \sum_s \beta_s B_s, \tag{27}$$

is a simple linear combination of the B_s's, and the coefficients β_s depend only on the geometry of the annuli. In particular, if we estimate B_s with $\hat{B}_s = N_s/A_s$, then we can estimate B_{src} with

$$\hat{B}'_{\mathrm{src}} = \sum_s \beta_s N_s/A_s, \tag{28}$$

where the prime indicates that this estimate of $B_{\rm src}$ is obtained from the surrounding annuli and not from the direct $N_{\rm src}/A_{\rm src}$. Note that the β_s's are not necessarily positive; thus, it is possible for equation (28) to produce a negative estimate of the background $B_{\rm src}$.

2.3.1. *An example: two concentric annuli*

Consider a source region $\mathcal{S}_{\rm src}$ surrounded by *two* concentric annuli: $\mathcal{S}_{\rm inner}$ and $\mathcal{S}_{\rm outer}$. See figure 2. If $B(x,y)$ can be accurately modeled as a cubic function of (x,y) in the region containing the annuli, then we can write

$$\begin{aligned} B_{\rm src} &= L_0 + L_1 r_{\rm src}^2 \\ B_{\rm inner} &= L_0 + L_1 r_{\rm inner}^2 \\ B_{\rm outer} &= L_0 + L_1 r_{\rm outer}^2 \end{aligned} \tag{29}$$

where L_0 and L_1 are two scalars which depend on the underlying cubic background function, and $r_{\rm src}$, $r_{\rm inner}$, and $r_{\rm outer}$ are the "average radii" of the center, inner, and outer annuli. This average is defined in terms of the second moment for each of the three areas:

$$r_{\mathcal{S}}^2 = R_{1,\mathcal{S}} = \frac{1}{2}\left(r_{i,\mathcal{S}}^2 + r_{o,\mathcal{S}}^2\right). \tag{30}$$

Here $r_{i,\mathcal{S}}$ is the inner radius, and $r_{o,\mathcal{S}}$ is the outer radius, of the annulus $\mathcal{S}$. We can now estimate the average count density for the central area as a linear combination of the count densities in each of the two surrounding annuli:

$$B_{\rm src} = \beta B_{\rm inner} + (1-\beta) B_{\rm outer} \tag{31}$$

with

$$\beta = \frac{r_{\rm outer}^2 - r_{\rm src}^2}{r_{\rm outer}^2 - r_{\rm inner}^2}. \tag{32}$$

We remark again that β depends only on the geometry of the the background annuli and the source region. It does not depend on the underlying background nonuniformity. Thus, having set up a geometrical configuration, one needs to compute β only once. We also remark that since $r_{\rm inner} > r_{\rm src}$, we have $\beta > 1$; this implies that the coefficient of $B_{\rm outer}$ is always negative. A "typical" value is $\beta = 1.5$ (and $1-\beta = -0.5$), which corresponds to the case that both annuli have the same area and are much larger than the hole in the inner annulus.

It is clear from equation (29) that a plot of B versus r^2 will produce a straight line. This provides a convenient visualization (as seen in figure 3) of the "linear extrapolation" of the background from the outer and inner rings to the central source region.

2.3.2. *Overdetermined case*

Although we need at least $1 + \lfloor q/2 \rfloor$ annuli to fit an order q polynomial, there is no reason not to use more than the minimum number of annuli. For the $q = 3$ case, we can imagine replacing the "linear extrapolation" in figure 3 with a linear fit; if we do it this way, however, we have to be careful about the Poisson bias (Wheaton et al. 1995). In general, we are free to choose our coefficients β_s however we like so long as the following conditions are met:

$$R_{\mathrm{src},k} = \sum_s \beta_s R_{s,k} \tag{33}$$

for $k = 0, \ldots, \lfloor q/2 \rfloor$. These conditions ensure that if the background varies as an order-q polynomial, then equation (27) will hold, and we will have an unbiased estimator. In later sections, we will discuss different approaches for optimizing the choice of the coefficients β_s.

It is useful to consider the limit of an infinite number of annuli, and to take the continuum limit. The role of the coefficients β_s is then played by a function $\beta(r)$ where r is the radius of the infintesimal annulus.[2] The estimator for the average background in the source region is given by an integral

$$\hat{B}'_{\mathrm{src}} = \int \beta(r) B(r) 2\pi r \, dr \tag{34}$$

but this can be more usefully written as a sum over all the individual counts (photons):

$$\hat{B}'_{\mathrm{src}} = \sum_{n=1}^{N} \beta(r_n) \tag{35}$$

where r_n is the distance[3] from the candidate point source location to the position of the n-th photon. The conditions to fit an order q polynomial are obtained by setting $B(r) = r^{2k}$ for $k = 0, \ldots, \lfloor q/2 \rfloor$, and employing equation (34) to obtain

$$\int \beta(r) 2\pi r^{2k+1} \, dr = R_{\mathrm{src},k}. \tag{36}$$

Note that in the limit as the radius of the source region goes to zero, we have $R_{\mathrm{src},k} = \delta_{k,0}$. In this limit, we are estimating the background density at a point, instead of estimating the average background over a region.

Equations (34,36) are written for circular annuli; essentially the same result can be applied for square annuli, but with '2π' (perimeter of unit circle) replaced by '8' (perimiter of unit-radius square).

The use of a continuum kernel for simultaneous point source detection and background subtraction is also possible (Damiani et al. (1997) use wavelets for this purpose). The optimal kernel can be constructed to match the point spread function of the telescope and at the same time be insensitive to polynomial background nonuniformity.

---

[2]Actually, the $\beta(r)$ that we will use is not exactly the continuum analog of β_s; it's more like $\beta(r) \sim \beta_s/A_s$.

[3]The distance is Euclidean ($r = \sqrt{x^2 + y^2}$) if we are using circular annuli – which we might as well do, if we have distances available as floating point numbers. The distance is given by the "maximum" metric ($r = \max(x, y)$) if we are using square annuli.

3. Error (variance and bias) in background estimation

In the limit as the background densities B_s are precisely known, the estimate of $B_{\rm src}$ given by equation (27) will be precise. In practice, however, these background densities are estimated from a finite number of counts in each of the annuli.

If there are N_s counts in an area A_s in the s-th annulus, then $\hat{B}_s = N_s/A_s$ is the estimated count density. And since these counts arise from a Poisson source, the average squared error in $\hat{B}_s$ will be given by

$$E_s^2 = \langle(\hat{B}_s - B_s)^2\rangle = B_s/A_s. \tag{37}$$

Using this expression, we can write the averaged squared error for our estimate in equation (28) of the count density in the source area as

$$E_{\rm src}^2 = \langle(\hat{B}'_{\rm src} - B_{\rm src})^2\rangle = \sum_s \beta_s^2 E_s^2 = \sum_s \beta_s^2 B_s/A_s \tag{38}$$

It is straightforward to extend this expression to the continuum limit:

$$E_{\rm src}^2 = \int \beta^2(r) B(r)\, 2\pi r\, dr. \tag{39}$$

where we define $B(r) \equiv \frac{1}{2\pi}\int_0^{2\pi} B(r,\theta)\, d\theta$.

The above equations express the *variance* in the estimate of background count density at the source location; in general, there will also be a *bias*. If the background is well fit by a polynomial of order q, then the bias is zero. One way to estimate this bias is to assume that the background is well-fit by an order q' polynomial, with $q' \geq q$. Then the bias in the order-q' multi-annulus estimator is zero, and the bias in the order-q estimator will be given by the difference between these two estimators. In general, using smaller values of q will increase the bias, but at the same time reduce the variance. Determining the optimal order q is therefore a trade-off between bias and variance. (In our experience, however, the optimal q is never larger than 3.)

3.1. Uniform background

For the moment, consider the case that the background is uniform (so that $B_s = B$ for all s). The bias in this case is zero, and only the variance is relevant. For the single annulus estimator, the variance is given by

$$V_1 = B/A \tag{40}$$

where $A = A_{\rm inner} + A_{\rm outer}$. For the two annulus estimator, we have

$$V_2 = \beta^2 B/A_{\rm inner} + (1-\beta)^2 B/A_{\rm outer} = \left(\frac{\beta^2}{\alpha} + \frac{(1-\beta)^2}{1-\alpha}\right) B/A \tag{41}$$

$$= \left(1 + \frac{(\alpha-\beta)^2}{\alpha(1-\alpha)}\right) B/A \tag{42}$$

where β is given by equation (32), and we have defined

$$\alpha = A_{\rm inner}/(A_{\rm inner} + A_{\rm outer}). \tag{43}$$

It it clear from these expressions that V_2 can never be smaller than V_1; in fact, from the geometrical constraint that the annuli and source region cannot overlap, it is not too hard to show that V_2/V_1 is always larger than five.[4]

Note that equation (42) provides a criterion for choosing an optimal partition of a background annulus into inner and outer annuli. When the background is uniform, it is straightforward to show that this optimum partition occurs when the areas of the inner and outer annuli are equal. In this case, $\alpha = 0.5$, and $V_2 = \left(1 + (2\beta - 1)^2\right) V_1$.

When the background is uniform, preference clearly goes to the one-annulus estimator, since it has substantially smaller variance. If we were to compute the variance for a three-annulus estimator which fit an order $q = 5$ polynomial to the background, we would find an even larger variance. On the other hand, using more than two annuli, but sticking to $q = 3$, will reduce the variance somewhat. This is most evident in the continuum limit.

In the continuum limit, there is a simple criterion for choosing the optimal function $\beta(r)$: minimize the variance in equation (39) while maintaining the constraints in equation (36). Using the method of Lagrange multipliers, and some variational calculus, one can show that the optimal function is of the form

$$\beta(r) = \frac{\sum_{k=0}^{\lfloor q/2 \rfloor} \lambda_k r^{2k}}{B(r)}. \tag{44}$$

where λ_k are constants whose values are determined from the conditions in equation (36) for $k = 0, \ldots, \lfloor q/2 \rfloor$.

As an example, consider the case that $B(r)$ is constant, that $q = 3$, and that the source region and annulus inner radius are both much smaller than the annulus outer radius. In that case, we have $\beta(r) = a + br^2$. The constraints in equation (36) become

$$\int_0^R \beta(r)\, 2\pi r\, dr = 2\pi \left(\frac{aR^2}{2} + \frac{bR^4}{4} \right) = 1 \tag{45}$$

$$\int_0^R \beta(r)\, 2\pi r^3\, dr = 2\pi \left(\frac{aR^4}{4} + \frac{bR^6}{6} \right) = 0 \tag{46}$$

and from these, we obtain

$$\beta(r) = \frac{4}{\pi R^2} - \frac{6}{\pi R^4} r^2. \tag{47}$$

[4]The factor of five is achieved in the limit as the inner radius of the inner annulus goes to zero, and $A_{\rm inner} = A_{\rm outer}$; we have $\beta = 1.5$, $\alpha = 0.5$ in this case, and then from equation (42), $V_2/V_1 = 5$.

as the optimal coefficient function. The variance of this optimal continuum estimator is

$$V_C = \int_0^R \beta^2(r)B(r)\,2\pi r\,dr \tag{48}$$

$$= 2\pi B \int_0^R \left[\frac{4}{\pi R^2} - \frac{6}{\pi R^4}r^2\right]^2 r\,dr = \frac{4B}{\pi R^2} = 4B/A. \tag{49}$$

We see that this value is four times larger than the single-annulus variance, but twenty percent smaller than the equivalent two-annulus variance. (See figure 4.)

3.2. Nonuniform background

While it is useful to understand the performance of the various estimators in the specical case of uniform background, the whole purpose of these multi-annulus estimators is to improve the characterization of nonuniform backgrounds. With nonuniform backgrounds, the bias is in general nonzero, and so bias/variance tradeoffs need to be considered.

For a two annulus estimator, if the background is nonuniform, then $B_{\rm inner} \neq B_{\rm outer}$ in general. Let

$$B = \alpha B_{\rm inner} + (1-\alpha)B_{\rm outer} \tag{50}$$

be the average background,[5] and let

$$\delta = \frac{B_{\rm inner} - B_{\rm outer}}{B} \tag{51}$$

be a measure of nonuniformity which is restricted to $-1 \le \delta \le 1$. Here, positive δ corresponds to a "peak" at the source location, and negative δ to a valley. Note that we can express arbitrary linear combinations of $B_{\rm inner}$ and $B_{\rm outer}$ in terms of the average background and this nonuniformity measure.

$$uB_{\rm inner} + vB_{\rm outer} = (u+v)B + ((1-\alpha)u - \alpha v)\delta B \tag{52}$$

If the background nonuniformity is well modeled by a cubic polynomial, then the bias in the two-annulus estimator will be zero; this means that the bias for the one annulus estimator is given by the difference between the one and two annulus estimators.

$$\begin{aligned}\langle \hat{B}'_{\rm src} - B_{\rm src}\rangle &= B - (\beta B_{\rm inner} + (1-\beta)B_{\rm outer}) \\ &= (\alpha B_{\rm inner} + (1-\alpha)B_{\rm outer}) - (\beta B_{\rm inner} + (1-\beta)B_{\rm outer}) \\ &= (\alpha-\beta)\delta B \end{aligned} \tag{53}$$

We can now write the total relative squared error (variance plus squared bias divided by B^2) for the one-annulus estimator:

$$T_1^2 = \frac{1}{\mathcal{N}} + (\alpha-\beta)^2\delta^2 \tag{54}$$

---

[5] B is also the source background that would be estimated by the one-annulus estimator. Recall α was defined in equation (43) in terms of the ratio of areas of the inner and outer annuli.

where $\mathcal{N} = AB$ is the expected number of counts in the background annulus.

For the two-annulus estimator, the bias is zero but the variance is given by

$$V_2 = \beta^2 B_{\rm inner}/A_{\rm inner} + (1-\beta)^2 B_{\rm outer}/A_{\rm outer} \tag{55}$$

Using equation (52) to expand the above sum, we can write an expression for the total relative squared error:

$$T_2^2 = V_2/B^2 = \left\{ \left(\frac{\beta^2}{\alpha} + \frac{(1-\beta)^2}{1-\alpha} \right) + \left(\frac{\beta^2(1-\alpha)}{\alpha} - \frac{(1-\beta)^2\alpha}{1-\alpha} \right) \delta \right\} \frac{1}{\mathcal{N}}. \tag{56}$$

If $|\delta| \ll 1$, we can write more simply

$$T_2^2 = \left(1 + \frac{(\alpha-\beta)^2}{\alpha(1-\alpha)} \right) \frac{1}{\mathcal{N}}. \tag{57}$$

One prefers the two-annulus method if $T_2^2 < T_1^2$, and this happens when

$$\mathcal{N}\delta^2 > \frac{1}{\alpha(1-\alpha)}. \tag{58}$$

The two-annulus estimator is preferred when the bias is large (δ large) and the variance is small ($\mathcal{N}$ large). If the background annuli cover a large area, then both of these conditions are more likely to hold.

When the background is nonuniform, the optimal partition of the background annulus into two annuli is no longer into equal areas. In general, local peaks ($\delta > 0$) prefer a larger inner annulus, and local valleys ($\delta < 0$) prefer a larger outer annulus. However, the gain for mild nonlinearities is not substantial, and since one usually prefers to use the same-sized annuli for the entire map, we recommend $A_{\rm outer} \approx A_{\rm inner}$ as a general rule of thumb.

3.3. Combination of one- and two-annulus methods

In comparing the one- and two-annulus methods, it is useful to recognize that both methods provide an estimate of $B_{\rm src}$ as a linear combination of $\hat{B}_{\rm inner}$ and $\hat{B}_{\rm outer}$, with the only difference being the choice of coefficients:

$$\hat{B}'_{\rm src} = \gamma \hat{B}_{\rm inner} + (1-\gamma)\hat{B}_{\rm outer}. \tag{59}$$

Here, $\gamma = \alpha$ with α defined in equation (43) produces the one-annulus estimator, and $\gamma = \beta$ with β defined in equation (32) gives the two-annulus estimator. Rather than try to make a dichotomous choice between the one- and two- annulus estimators, we can instead ask about the optimal choice of γ. In principle, it is straightforward to derive the optimum; we have

$$T_\gamma^2 = \left\{ \left(1 + \frac{(\alpha-\gamma)^2}{\alpha(1-\alpha)} \right) + \left(\frac{\gamma^2(1-\alpha)}{\alpha} - \frac{(1-\gamma)^2\alpha}{1-\alpha} \right) \delta \right\} \frac{1}{\mathcal{N}} + (\gamma-\beta)^2\delta^2, \tag{60}$$

so for a given $\mathcal{N}$ and δ, we can take a derivative and set it to zero. Using the $\delta \ll 1$ approximation, this produces:

$$\gamma_{\rm optimal} = \frac{\alpha + \zeta\beta}{1+\zeta} \tag{61}$$

where $\zeta = \mathcal{N}\delta^2\alpha(1-\alpha)$. Note that this expression for the optimal γ depends on $\mathcal{N}$ and δ, which will vary over different parts of the map. There are two approaches we can take in this situation. One is to develop an "adaptive" formula for γ that varies with position on the map; its value will depend on local properties of the map, which will have to be estimated at each position. A second approach is to find a single best γ for the entire map.

3.3.1. Adaptive linear combination

The simplest adaptive linear combination of $B_{\rm inner}$ and $B_{\rm outer}$ uses the expression for γ in equation (61), but this requires an estimate of the nonuniformity δ. A natural estimator (following equation (51)) takes $\hat{\delta} = (\hat{B}_{\rm outer} - \hat{B}_{\rm inner})/\hat{B}$, but this will generally overestimate δ^2, which will make γ larger than optimal. Roughly,

$$\langle(\hat{\delta})^2\rangle \approx \delta^2 + \frac{1}{\alpha(1-\alpha)\mathcal{N}} \tag{62}$$

which suggests using $\widehat{\delta^2} = (\hat{\delta})^2 - \frac{1}{\alpha(1-\alpha)\mathcal{N}}$; in other words, use equation (61) with

$$\zeta = \max\left\{0,\ \frac{A_{\rm inner}A_{\rm outer}(\hat{B}_{\rm outer} - \hat{B}_{\rm inner})^2}{(A_{\rm inner} + A_{\rm outer})\hat{B}} - 1\right\}. \tag{63}$$

3.3.2. Average best linear combination

Although the adaptive estimate of γ in the previous section should in principle be the most accurate (at least for high enough count densities), we have obtained better estimates using a single "average best" γ. Let $\hat{B}_{\rm src}$ denote the estimated counts per pixel in the source area using the actual counts in the source area:

$$\hat{B}_{\rm src} = \frac{N_{\rm src}}{A_{\rm src}} \tag{64}$$

and let $\hat{B}'_{\rm src}$ be the estimated counts per pixel in the source area as estimated from the counts in the background annuli. If there is not a point source at the candidate location, then both estimates should roughly agree. Let

$$\Delta\hat{B}_{\rm src} = \hat{B}_{\rm src} - \hat{B}'_{\rm src} \tag{65}$$

be the extent to which they do not agree. Note that $\Delta\hat{B}_{\rm src}$ is a difference of two *estimators*; it is a quantity that can be computed directly from a map without any knowledge of the actual background $B_{\rm src}$.

This empirical estimate of estimation error can be combined with equation (59) to produce a tool for choosing a single "average best" parameter γ. Note that

$$\Delta\hat{B}_{\rm src} = \hat{B}_{\rm src} - \Big(\gamma\hat{B}_{\rm inner} + (1-\gamma)\hat{B}_{\rm outer}\Big) \tag{66}$$

and

$$\langle(\Delta\hat{B}_{\rm src})^2\rangle = \langle(\hat{B}_{\rm src} - \hat{B}_{\rm outer})^2\rangle - 2\gamma\langle(\hat{B}_{\rm src} - \hat{B}_{\rm outer})(\hat{B}_{\rm inner} - \hat{B}_{\rm outer})\rangle + \gamma^2\langle(\hat{B}_{\rm inner} - \hat{B}_{\rm outer})^2\rangle \tag{67}$$

and this is a simple quadratic equation whose minimum occurs at

$$\gamma_{\rm optimal} = \frac{\langle(\hat{B}_{\rm src} - \hat{B}_{\rm outer})(\hat{B}_{\rm inner} - \hat{B}_{\rm outer})\rangle}{\langle(\hat{B}_{\rm inner} - \hat{B}_{\rm outer})^2\rangle}. \tag{68}$$

Since this expression uses $\hat{B}_{\rm src}$ which is estimated by counting photons in the source region, this estimate of $\gamma_{\rm optimal}$ will only be useful in a map that does not have a lot of real sources. If there are a few bright sources, these should be masked off in the estimate of $\gamma_{\rm optimal}$; if there are many sources, then one must iteratively find, fit, and subtract off the real sources. The difficulties involved in this source-confused regime are beyond the scope of this article.

4. Applications of multiple annuli

We will illustrate a number of practical uses for multiple annulus background estimation on a real ALEXIS data set (figure 1a) and on an artificial data set (figure 1b) which has a cubic polynomial background and five artifical point sources. Four different applications of multiple annulus methods will be provided: estimating background level; detecting point sources; generating surrogate maps for estimating false alarm rates; and quantifying background nonuniformity.

4.1. Estimating background level

In comparing various geometries of single and multiple annulus estimators, it is useful to have an index that measures the accuracy of these estimators directly from the data. In Section 3.3.2, we introduced an expression $\Delta\hat{B}_{\rm src} = \hat{B}_{\rm src} - \hat{B}'_{\rm src}$ which describes the difference between two estimates of the background in a source region. The first ($\hat{B}_{\rm src}$) is a direct estimate from counts in the source region and the second ($\hat{B}'_{\rm src}$) is an indirect estimate obtained from annular regions that do not include the source region. In the absence of a real point source, we can evaluate the quality of the indirect annular estimate by comparing it to the direct estimate.

Although we can compute $\Delta\hat{B}_{\rm src}$ directly from the data, it is useful to note that we can write this as a difference of differences:

$$\Delta\hat{B}_{\rm src} = (\hat{B}_{\rm src} - B_{\rm src}) - (\hat{B}'_{\rm src} - B_{\rm src}) \tag{69}$$

where $B_{\rm src}$ is the true (but unknown) background. This suggests that there are two contributions to the total variance in $(\Delta\hat{B}_{\rm src})^2$: a source fluctuation and a background estimation error.

The background estimation error itself arises from two causes: the actual bias arising from the assumption that the background is a low-order polynomial, and the Poisson fluctuations in the counts in the annular regions. Both of these are independent of the source fluctuation error (which is due only to the Poisson fluctuation in the counts in the source region), so these two contributions to the variance (source fluctuation and background estimation error) are independent, and we can write:

$$\langle(\Delta\hat{B}_{\rm src})^2\rangle = \langle(\hat{B}_{\rm src} - B_{\rm src})^2\rangle + \langle(\hat{B}'_{\rm src} - B_{\rm src})^2\rangle. \tag{70}$$

with equality holding when $\langle\cdot\rangle$ denotes a true ensemble average. We can furthermore estimate the first term (the source fluctuation error) from the result in equation (37):

$$\langle(\hat{B}_{\rm src} - B_{\rm src})^2\rangle = B_{\rm src}/A_{\rm src} \approx \hat{B}_{\rm src}/A_{\rm src}. \tag{71}$$

This gives an expression for the background estimation error:

$$\langle(\hat{B}'_{\rm src} - B_{\rm src})^2\rangle \approx \langle(\Delta\hat{B}_{\rm src})^2\rangle - \hat{B}_{\rm src}/A_{\rm src}. \tag{72}$$

Dividing by the source fluctuation error, we can obtain a directly computable dimensionless quantity that we call the "empirical background error index":

$$\mathcal{E} = \frac{\langle(\Delta\hat{B}_{\rm src})^2\rangle}{\langle\hat{B}_{\rm src}\rangle/A_{\rm src}} - 1 \tag{73}$$

which is essentially the ratio of the average background estimation error to the average source fluctuation error. A smaller value is better, though there is arguably a point of diminishing returns in obtaining a value very much less than one.

In figure 5 (resp. figure 6), we compare the empirical background error index for one- and two-annulus estimators as a function of outer annulus diameter for the ALEXIS (resp. artificial cubic background) map. For small annuli, the bias is smaller but the variance is larger, and preference goes to the one-annulus estimator which minimizes the variance. For larger annuli, the bias is larger but the variance is smaller, and preference goes to the two-annulus estimator, which minimizes bias at the expense of variance. For intermediate-sized annuli, the optimal estimator is a linear combination of the one and two annulus estimator. These are only qualitative trends; quantitative values (*e.g.,* optimal linear coefficients, or optimal annulus size) depend on the background. What the empirical background error index provides is a way to estimate these quantitative values directly from the raw data.

4.2. Detecting point sources

Our main motivation in attempting to more accurately estimate the background is that this provides a more sensitive point source detections – in particular, it permits us to detect weaker real sources without increasing the false detection rate.

When the background is known exactly, it is straightforward to assess the significance of a given point source candidate. If $N_{\rm src}$ counts are observed in the source region, and the background

$B_{\rm src}$ is known exactly, then $S = N_{\rm src} - A_{\rm src}B_{\rm src}$ estimates the source strength. Under the null hypothesis, the quantity $N_{\rm src}$ will be Poission distributed with mean $A_{\rm src}B_{\rm src}$; the variance of $N_{\rm src}$ (and therefore of S) will also be $A_{\rm src}B_{\rm src}$, so the "signal to noise ratio" will be given by

$$S/N = \frac{S}{\sqrt{\mathrm{Var}(S)}} = \frac{N_{\rm src} - A_{\rm src}B_{\rm src}}{\sqrt{A_{\rm src}B_{\rm src}}}. \tag{74}$$

Under the null, S/N will have mean zero and variance one.[6] If the count rate is high, then S/N will furthermore be distributed as a Gaussian, and therefore it makes sense to think of the S/N as a number of "sigmas of significance" for a given point source detection. For small numbers of counts, the Gaussian approximation becomes inaccurate, and the statistic S/N is not sufficient to characterize the significance of the point source detection. In that case, however, an exact test, using Poisson statistics, is straightforward to derive. Gehrels (1986), for instance, provides tables and useful approximations for the Poisson formulas that arise in this context. Zepka, Cordes, & Wasserman (1994) argue for using a histogram to characterize the background; this avoids assumptions of Gaussian or even Poisson statistics, but requires that that the background be uniform over a large enough region that a good histogram can be acquired.

But our interest is in the case that the background is not known, and must be estimated by counts in surrounding annuli. If the background is estimated by $\hat{B}'_{\rm src}$, then the signal is given by $S = N_{\rm src} - A_{\rm src}\hat{B}'_{\rm src}$, and the "noise" has an extra contribution due to the variance of the estimator. In particular, for the multiple-annulus estimators, we can write

$$S = N_{\rm src} - A_{\rm src}\sum_s \beta_s N_s/A_s \tag{75}$$

and the variance is given by

$$\mathrm{Var}(S) = A_{\rm src}B_{\rm src} + A_{\rm src}^2 \sum_s \beta_s^2 B_s/A_s \tag{76}$$

where N_s (resp. A_s) is the counts (resp. area) in the s'th annulus. A more sensitive statistic would employ a matched filter (see Vikhlinin et al. (1995) for a more extensive exposition on the use of a matched filter for source detection, a flat annulus for background subtraction, and Monte-Carlo tests for calibration).

The more precisely we can estimate the background, the more sensitive is our test for point source candidates; in particular, anything that can be done to reduce this variance (*e.g.,* using background annuli with large area A_s) will increase the statistical significance of any real sources, without altering the false alarm rate. This is a tangible motivation for estimating the background as precisely as possible.

However, exact values of $B_{\rm src}$ and B_s are not known in general, so the variance itself must be estimated. For the one-annulus estimator, a number of authors have shown how this should be done. In particular, Li & Ma (1983) argue (and demonstrate numerically as well) that one should use the

[6]Note that we do not use $\sqrt{N_{\rm src}}$ in the denominator, as some authors recommend. If we did, then S/N would not have mean zero and variance one under the null hypothesis.

null hypothesis that the background is uniform, and estimate $\hat{B} = (N_{\rm src} + N_{\rm back})/(A_{\rm src} + A_{\rm back})$. That is,

$$\mathrm{Var}(S) \approx A_{\rm src}\hat{B} + A_{\rm src}^2 \hat{B}/A_{\rm back} = (A_{\rm src}/A_{\rm back})(N_{\rm src} + N_{\rm back}) \tag{77}$$

and

$$S/N = \frac{N_{\rm src} - (A_{\rm src}/A_{\rm back})N_{\rm back}}{\sqrt{(A_{\rm src}/A_{\rm back})(N_{\rm src} + N_{\rm back})}}. \tag{78}$$

This statistic will have mean zero and variance one as long as the background is flat ($B_{\rm src} = B_{\rm back}$) and there are no point sources. It is only approximately Gaussian, however, and the approximation becomes poorer as the number of counts becomes small. Li & Ma (1983) also provide a much more complicated estimate of S/N which is more accurately Gaussian with lower counts. This more complicated expression can be further extended to account for weighted counts (Theiler & Bloch 1997a). The Cash statistic (Cash 1979; Nousek & Shue 1989) provides a good tool for parameter estimation and confidence intervals even when the number of counts in individual bins is small, but it is not really designed for point source detection. Damiani et al. (1997) employ a wavelet-based point source detector, essentially a continuum circular source kernel and annular background, and provide an empirical correction to Gaussian statistics with coefficients determined from a set of Monte-Carlo runs.

In Lampton (1994), the essentially binomial character of the counts in the source and background regions is exploited to produce an exact expression for statistical significance of counts in a source and background region. An extension of these exact results to nested annuli is described in Theiler & Bloch (1997b). Interestingly, Lampton's formula is equivalent to one derived earlier in Alexandreas et al. (1993), but the earlier derivation is based on an entirely different approach.

But all of these exact results and corrections to Gaussian statistics assume a uniform background. For the nonuniform background, at least for the purposes of this study, we will employ the implicit Gaussian assumption in our use of signal to noise (or "sigmas") to characterize significance. However, in the next section, we will describe an empirical approach for calibrating these sigmas to actual significance.

The "signal" and "noise" for the multiple-annulus estimators are given in equation (75) and equation (76). As with the one-annulus estimator, the signal depends only on the counts in and the areas of the source region and background annuli, but the noise depends on the true background levels. To keep things simple, we will follow the approach of Li & Ma (1983), and use $\hat{B} = N_{\rm total}/A_{\rm total}$ where $N_{\rm total} = N_{\rm src} + \sum_s N_s$ and $A_{\rm total} = A_{\rm src} + \sum_s A_s$; then

$$\mathrm{Var}(S) = N_{\rm total}(A_{\rm src}/A_{\rm total}) \left(1 + A_{\rm src}\sum_s \beta_s^2/A_s\right) \tag{79}$$

and we measure significance with

$$S/N = \frac{N_{\rm src} - A_{\rm src}\sum_s \beta_s N_s/A_s}{\sqrt{N_{\rm total}(A_{\rm src}/A_{\rm total})\left(1 + A_{\rm src}\sum_s \beta_s^2/A_s\right)}}. \tag{80}$$

In figure 7, we show maps of the significance S/N for the ALEXIS data, as estimated using one- and two-annulus methods. A number of bright O and B stars and previously identified bright extreme ultraviolet sources (Bowyer et al. 1996) are readily identifiable, as well as others that may be unidentified transient sources or false alarms; a more detailed study of these detections will be reported in a later paper. Table 1 shows all sources that are detected at the four sigma level using one of the two methods. For those significant at the five sigma level, identifications are provided as well. For these identified sources, there is a fairly close correspondence between the significance level of the two methods, though the two-annulus detector is usually the more significant.

In figure 8, we show significance maps for the cubic background map, again using one- and two-annulus methods. Point 1, the lower left artificial point source that is at the bottom of the trough, is barely detected by the one-annulus method with a significance of just above 3.0. From the figure, it also appears that the one-annulus detector exhibits a spatially uneven number of false alarms, with most of the false alarms occuring in the upper right quadrant where the background has a peak. By contrast, the two-annulus method produces false detections that are spread more evenly over the map, and the real source in the lower left quadrant is more readily identified.

To study this effect more systematically, we repeated this experiment a thousand times, and the results are shown in Table 2. The two-annulus detector was slightly better, on average, than the one-annulus detector for points 2, 4, and 5; these are points on the diagonal where the background curvature is small. The two-annulus detector was substantially better for point 1, which is in the the trough. The one-annulus detector reported a larger sigma for point 3, the upper right point source, but that is also where the one-annulus detector has its highest false alarm rate. In fact, the one-annulus detector reported an average significance (4.2 sigmas) for this point that was larger than the nominal significance (4.0 sigmas) that was designed into the experiment.

4.3. Generating "surrogate maps"

It is sometimes possible to analytically characterize the false alarm rate (or p-value) for simple point source detection algorithms when applied to a single candidate point source; but it is generally a lot more complicated, and often is outright intractable, to obtain false alarm rates for entire maps. In general, one discounts the significance of a candidate point source by the number of independent point source detection attempts (or "trials"). But when the source regions and background annuli act as "moving windows" over the map, the detection attempts are not independent, and it is nontrivial to get the correct trials factor. Saja (1995) has discussed the spatial overlapping window problem, and has computed (by numerical integration) the "completeness" versus "spurious detection rate" for a given magnitude limit and signal to noise ratio. Biller et al. (1994) look at the simpler case of overlapping time windows, and provide an empirical fit to the trials factor (see Table 3 of that reference). See Biller (1996) for a more extensive discussion of trial factors in the context of combining statistical tests in an open-ended search. If the background is known precisely, and the sources are sufficiently rare, the problem can be treated analytically (Politzer & Preskill 1986), but for our unknown and spatially nonuniform backgrounds, we resort to Monte-Carlo calculation.

If we have a good estimate of the background at each pixel, we can can make an ensemble of "surrogate maps" by assigning each pixel a value chosen from a Poisson distribution with mean equal to the background at the pixel. The surrogate maps, by definition, do not have point sources, so any point source detections will be spurious. Applying the point source detection algorithm to a large number of such maps, one can estimate of the false alarm rate, and in particular, can find an appropriate threshold for the "number of sigmas" of significance a single source must exhibit to be significant at a given level for the entire map.

The most straightforward way to estimate the background at each pixel is to use a one or two annulus estimator, as we have discussed in earlier sections. However, this generates a background map which is not smoothly varying from pixel to pixel, but instead includes fluctuation that arises from the Poisson statistics in the original map. Such surrogates generate more false alarms than are consistent with the null hypothesis of a smoothly varying background.

Our approach for generating surrogate maps is to find a background function $B(x, y)$ which is as smooth as possible while still being consistent with the original map. We can define "smoothness" in terms of the two-annulus estimator. A "perfectly smooth" map is one that can be modeled exactly as a cubic polynomial; such a map will satisfy

$$B_{ij} = \beta B_{\text{inner}} + (1-\beta) B_{\text{outer}} \tag{81}$$

where B_{inner} and B_{outer} are averages of B_{ij} over the inner and outer annuli, and β is given by equation (32). Exact equality is an unreasonable demand, because that implies a single cubic polynomial fit over the entire background. However, we can try to satisfy this equality as closely as possible, while constraining the background to be consistent with the data. In particular, we want

$$\left\langle \frac{(N_{ij} - B_{ij})^2}{B_{ij}} \right\rangle \approx 1. \tag{82}$$

To find a B_{ij} which simultaneously satisfies both (approximate) constraints, we take an iterative approach:

1. On the first iteration, we estimate B_{ij} at each pixel using the "average best" linear combination of two annuli described in Section 3.3.2.

2. On subsequent iterations, we refine this estimate of B_{ij} using the straight two-annulus method as defined in equation (31) and equation (32).

3. For each of these subsequent iterations, however, we perturb our estimate by a small fraction ϵ so that it does not stray too far from the data. That is,

$$B_{ij}^{(n+1)} = (1-\epsilon)\left(\beta B_{\text{inner}}^{(n)} + (1-\beta) B_{\text{outer}}^{(n)}\right) + \epsilon N_{ij}. \tag{83}$$

   In our implementation, the ϵ is adjusted in an *ad hoc* manner until equation (82) is satisfied; it is not difficult to imagine ways to automate this selection.

This background map is computed just once; multiple surrogate maps are generated by replacing each pixel of the background map with an integer chosen randomly from a Poission distribution with mean equal to the floating point background value. Figure 9 shows the results of one thousand surrogate maps; for each map, the point source algorithm is applied, and the statistics of point source detections (which by definition are all spurious) are maintained in a cumulative histogram.

This histogram provides a calibration which tells how many spurious detections are expected in the map as a function of "sigmas of significance" for a single detection. The dotted lines in figure 9 indicate the required number of sigmas for a single source detection in order to achieve the traditional level of p=0.05 significance for the entire map. For the ALEXIS map, this value is 5.0 sigmas; for the artifical map, it is about 4.6 sigmas.

From this calibration, we can compare the false alarm rates of the one and two annulus detectors. For the ALEXIS data, as seen in figure 9a, there is little difference between the two. There is a discernible difference for the artificial cubic background map; as shown in figure 10a, the one-annulus method produces approximately 20% more false alarms. This is not in itself a problem for the one-annulus detector, since the important thing is that the false alarm rate can be estimated; one simply adjusts the level of S/N that is needed for a confident detection. More worrying is that fact that the one-annulus method's false alarms do not occur uniformly in the map; if we restrict our attention to the upper right quadrant (where the background is generally peaked), then figure 10b shows that the false alarm rate for the one-annulus method is roughly double that of the two-annulus method.

Since we know the true background for the artificial map, we can use this to asses how well the surrogate maps estimate the true false alarm rates. To estimate these true rates, we performed a Monte-Carlo experiment with one thousand realizations of the artificial cubic background map, but without any point sources added, and applied the one-annulus and two-annulus detectors to these realizations. Figure 11 shows the ratio of the false alarm rate estimated from the surrogate maps to the true false alarm rate estimated from the Monte-Carlo experiment. This ratio is very nearly one (to within estimation error) for the one-annulus detector, and within a few percent of one for the two-annulus detector. That the surrogate maps provide a slightly higher false alarm rate leads to slightly more conservative point source detections in the real map.

4.4. Characterizing background nonuniformity

Although the multiple and continuum annuli estimators can account for smooth (polynomial) background nonuniformity when the count density is not too low, there are still times when a single-annulus estimator is preferred. As we've seen, a single-annulus estimator has lower variance than a multiple-annulus estimator. Under the assumption of uniform background, one can furthermore obtain an exact test of significance (*e.g.,* Lampton 1994), even for arbitrarily low counts. But even in this single-annulus scenario, it is useful to check the assumption of background uniformity.

One natural measure, which was originally used on the ALEXIS project, is the Poisson dispersion index (Freund & Williams 1966). If N_i is the count in the i-th pixel in the background annulus, and there are a total of K pixels, then the statistic

$$X = \frac{\sum_{i=1}^{K}(N_i - \overline{n})^2}{\overline{n}} \tag{84}$$

where $\overline{n} = \sum_i N_i/K = N/K$ is the average counts per pixel, will be approximately chi-square distributed with $K-1$ degrees of freedom. If X is large ($X \gg K-1$), that indicates a pixel-to-pixel nonuniformity that is larger than can be accounted for by Poisson variation.

This statistic is less than ideal from the point of view of point source detection for several reasons. Since there is no spatial information coded into the statistic, it is only sensitive to pixel-by-pixel variations. This makes it relatively insensitive to a weak nonuniformity that is spread over a large area; this is a problem that is exacerbated when the pixels are small. A related small-pixel problem occurs when there are many more pixels than photons (when $\overline{n}$ is much less than one). In this regime, the distribution of X is no longer expected to be chi-square. In fact, in the limit as $\overline{n} \to 0$, each pixel will contain either zero photons or one, and $X = (K^2 - N^2)/N$ regardless of how those photons are arranged.

On the other side of the coin, the Poisson dispersion index is sensitive to all kinds of deviations from uniformity, including those, such as a linear gradient, for which a single-annulus estimator is quite adequate (is optimal in fact) for estimating the background in the source area. The statistic will (correctly) indicate that the background is nonuniform, but a perfectly good background estimate will be needlessly disqualified.

Using concentric annuli, we will develop a statistic that is both more sensitive to weak quadratic nonuniformities and at the same time insensitive to such "benign" nonuniformities as linear gradients (or any odd polynomial powers).[7] We will define a statistic which is a simple linear function of the counts in the annuli:

$$T = \sum_s \eta_s N_s \tag{85}$$

where the coefficients η_s are chosen to satisfy the conditions

$$\sum_s \eta_s A_s = 0, \tag{86}$$

$$\sum_s \eta_s^2 A_s / \sum_s A_s = 1. \tag{87}$$

This statistic will have mean zero, and variance $\langle T^2 \rangle = N$, where $N = \sum_s N_s$ is the total number of counts. In particular, we will be able to reject the null hypothesis of uniform background with $T/\sqrt{N}$ "sigmas" of significance. If there are two annuli, then there is only one solution for η_s: $\eta_{\rm inner} = \sqrt{(1-\alpha)/\alpha}$, and $\eta_{\rm outer} = \sqrt{\alpha/(1-\alpha)}$. For more than two annuli, we note, without going into detail, that it is possible to choose the coefficients η_s so that the statistic is optimally sensitive to quadratic nonuniformities – these are the nonuniformities that lead to the most serious mis-estimates of background when the single annulus estimator is used (a continuum-limit statistic, in which the coefficients η_s are replaced by a function $\eta(r)$, is also straightforward to derive). Figure 12 compares the Poisson dispersion index and a two-annulus statistic, showing that the two-annulus statistic is completely insensitive to to linear gradients, but is more sensitive to weak quadradic nonuniformities.

The last two columns of Table 2 show how the annulus-based background statistic is able distinguish troughs (negative value at point 1), peaks (positive value at point 3), and low curvature

[7] Actually, it is not a bad idea to directly employ the Poisson dispersion index in equation (84), but with annular regions in place of individual pixels. If the regions have different areas, then a slight modification is needed, but such a statistic is by design insensitve to linear gradients, and since annular regions are generally much larger than individual pixels, one expects the chi-squared approximation to be more accurate.

points (2, 4, and 5) in the background nonuniformity. As with ordinary point source detection, there is a trade in the choice of annulus size. Choosing an outer annulus equal in size to the annulus that is used for point source detection provides an appropriately local measure of nonuniformity; choosing a larger annulus size however provides a more sensitive measure.

In the special case that there are two background annuli, then the distribution of $(N_{\text{inner}}, N_{\text{outer}})$ is binomial and an exact p-value can be computed in terms of the incomplete beta function. This was pointed out by Lampton (1994) in the context of determining whether the counts in a source region are consistent with the counts in a single background annulus. In particular, a one-sided p-value is given by the probability of seeing N_{inner} or more counts in the inner annulus.

$$p = \sum_{n=N_{\text{inner}}}^{N} \binom{N}{n} \alpha^n (1-\alpha)^{N-n} \equiv I_\alpha(N_{\text{inner}}, N_{\text{outer}}+1) \qquad (88)$$

where $N = N_{\text{inner}} + N_{\text{outer}}$, and $\alpha = A_{\text{inner}}/(A_{\text{inner}} + A_{\text{outer}})$, and I_α is the incomplete beta function. The one-sided p-value will be small when N_{inner} is unusually large; this occurs when the background is "peaked" near the candidate point source location, the very nonuniformity that is most likely to lead to a spurious point source detection.

We remark that this statistic does not "assume" that the background is smoothly varying, or well-modeled by a polynomial. It is simply a test of the null hypothesis that the background is uniform. It will detect many different kinds of deviations from uniformity, but is designed to be particularly powerful against case that the background has a smooth convexity (or "peakiness").

5. Conclusion

We have derived linear multiple-annulus estimators that provide unbiased background estimation when the background is spatially nonuniform but smoothly varying. The approach works for both circular and square background annuli, and can be conveniently applied to photon event lists as well as to maps of the sky with photons binned into square pixels. One trades accuracy for precision (lower bias for increased variance) in going to a multiple-annulus estimator, and if the count rate is low or if the background is nearly uniform, the trade becomes unfavorable. Fortunately, one does not have to depend on general trends or asymptotic results to inform this trade; the empirical background error index, described in Section 4.1, provides a simple figure of merit that can be computed directly from the data. As well as comparing distinct background estimation methods, it can be used to define an optimal annulus size and/or an optimal linear combination of the one and two annulus estimators.

We have seen that multiple-annulus background estimators can, in some cases at least (*e.g.,* the cubic background map), provide more robust point source detection. But if the count density in the map is not very high, the increased variance of the multiple-annulus estimators may lead to a preference for simple one-annulus point source detection. But even in this regime, multiple-annulus methods can play a supporting role. We have shown how a multiple-annulus smoothness condition can be used to generate nonuniform "surrogate maps" which are can be used for assessing false detection rates and significance thresholds. We have also shown how to use multiple annuli to characterize the nonuniformity of the background; potential point sources that are detected at places on the sky map with a high degree of nonuniformity will be more suspicious than those that are detected in flatter regions.

At this writing, the ALEXIS satellite is still flying, and is still taking data. The ALEXIS daily point source detection effort is described by Roussel-Dupré et al. (1996). As the mission nears completion, work is in progress on a final point source catalog.

Acknowledgements

We are grateful to all the dedicated ALEXIS operators who showed up at all hours of the day and night to tend satellite downlinks, for providing inspiration and data to the ten o'clock scholars who wrote this paper. We are particularly thankful to Diane Roussel-Dupré for numerous helpful suggestions on various aspects of this project and of this manuscript.

This work was conducted under the auspices of the United States Department of Energy.

REFERENCES

Alexandreas, D. E., et al. 1993, Nucl. Instr. Meth. Phys. Res. A, 328, 570

Biller, S., et al. 1994, ApJ, 423, 714

Biller, S. D. 1996, Astroparticle Phys., 4, 285

Bloch, J., et al. 1993, BAAS, 183, #13.10

Bloch, J., et al. 1994, in Proceedings of SPIE, Vol. 2280, EUV, X-Ray, and Gamma-Ray Instrumentation for Astronomy V, ed. O. H. W. Siegmund & J. V. Vallerga, 297

Bowyer, S., Lampton, M., Lewis, J., Wu, X., Jelinsky, P., & Malina, R. F. 1996, ApJS, 102, 129

Cash, W. 1979, ApJ, 228, 939

Damiani, F., Maggio, A., Micela, G., & Sciortino, S. 1997, ApJ, 483, 350

Freund, J. E., & Williams, F. J. 1966, Dictionary/Outline of Basic Statistics (New York: McGraw-Hill), Republished by Dover, New York, 1991

Gehrels, N. 1986, ApJ, 303, 336

Greisen, E. W., & Calabretta, M. 1995, in ASP Conference Series, Vol. 77, Astronomical Data Analysis Software and Systems IV, ed. R. A. Shaw, H. E. Payne, & J. J. E. Hayes (San Francisco: ASP), 233

Greisen, E. W., & Calabretta, M. 1996, "Representations of Celestial Coordinates in FITS," Preprint available at `http://fits.cv.nrao.edu/documents/wcs/wcs.html`

Lampton, M. 1994, ApJ, 436, 784

Li, T.-P., & Ma, Y.-Q. 1983, ApJ, 272, 317

Nousek, J. A., & Shue, D. R. 1989, ApJ, 342, 1207

Politzer, H. D., & Preskill, J. P. 1986, Phys. Rev. Lett., 56, 99

Priedhorsky, W. C., et al. 1988, in Proceedings of SPIE, Vol. 982, X-ray Instrumentation in Astronomy II, ed. L. Golub, 188

Psiaki, M. L., Theiler, J., Bloch, J., Ryan, S., Dill, R. W., & Warner, R. E. 1997, Journal of Guidance, Control, and Dynamics, 20, 1033

Roussel-Dupré, D., Bloch, J. J., Theiler, J., Pfafman, T., & Beauchesne, B. 1996, in ASP Conference Series, Vol. 101, Astronomical Data Analysis Software and Systems V, ed. G. H. Jacoby & J. Barnes (San Francisco: Astronomical Society of the Pacific), 112

Saja, P. 1995, AJ, 110, 916

Theiler, J., & Bloch, J. 1997a, in ASP Conference Series, Vol. 125, Astronomical Data Analysis Software and Systems VI, ed. G. Hunt & H. E. Payne (San Francisco: Astronomical Society of the Pacific), 151

Theiler, J., & Bloch, J. 1997b, in Statistical Challenges in Modern Astronomy II, ed. E. D. Feigelson & G. J. Babu (New York: Springer-Verlag), 407

Vikhlinin, A., Forman, W., Jones, C., & Murray, S. 1995, ApJ, 451, 542

Wheaton, W. A., Dunklee, A. L., Jacobsen, A. S., Ling, J. C., Mahoney, W. A., & Radocinski, R. G. 1995, ApJ, 438, 322

Zepka, A. F., Cordes, J. M., & Wasserman, I. 1994, ApJ, 427, 438

This preprint was prepared with the AAS LaTeX macros v4.0.

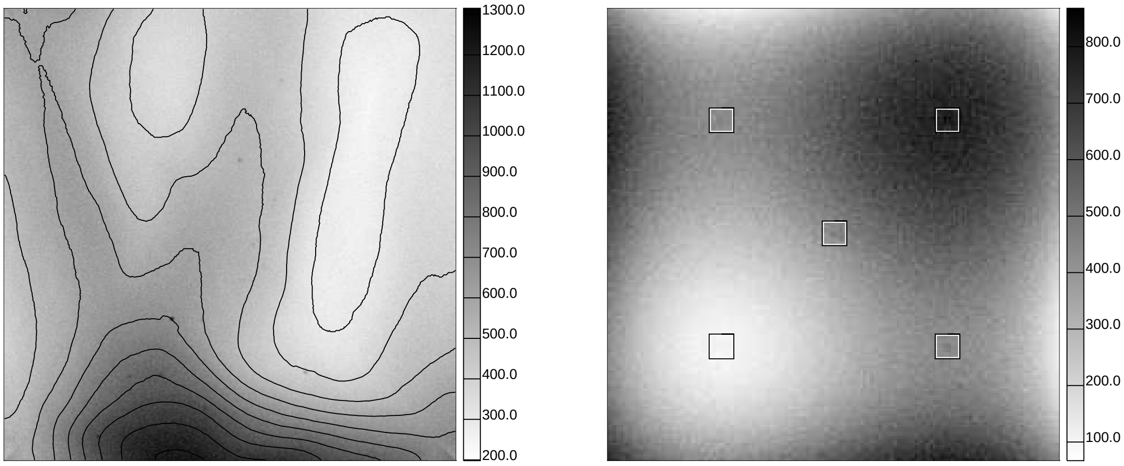

Fig. 1.— **(a)** This data set constitutes one face, centered at 90^o Right Ascension, and 0^o Declination, of the quadrilateralized spherical cube projection of a full-sky map generated by co-adding 49 months of raw count data from one of the six ALEXIS telescopes. The telescope we chose (1B), has a high signal to noise ratio compared to the other telescopes, and detects extreme ultraviolet photons in a narrow band centered at 172Å. The brightest object in this view is Sirius B, the white dwarf companion of the visibly brightest star in the sky; it is in the lower left quadrant, but is not easy to see before subtracting the background. The contour lines indicate the irregular, but relatively smooth, spatial nonuniformity of the background; most of this nonuniformity is due to the uneven exposure of the scanning telescope. To avoid edge effects, the 360×360 map has been extended by 50 pixels in each direction by including pixels from the four adjacent faces, and the corners have been filled in by reflecting pixels across the edges. The padded pixels are used only for background annuli; the point sources are only detected in the original quad-cube face. **(b)** An artificial data set was generated to have an exactly cubic polynomial background. Five artificial point sources were added at locations on the map indicated by the enclosing squares. All five have a source strength that would be significant at 4 sigmas, if the background were precisely known. The points are arranged like the five dots on a die, and each "point" is in fact a 3x3 source region with weight 0.2 in the center and 0.1 at each of the eight surrounding pixels. In this 200×200 map, the outer 30 pixels are reserved for "padding;" points are detected only in the interior.

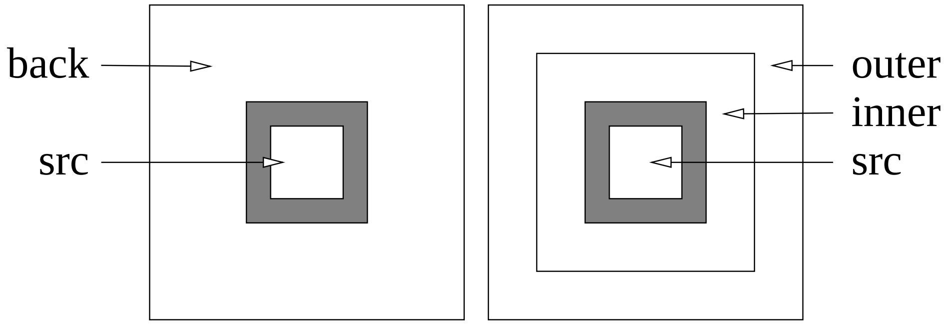

Fig. 2.— The one-annulus method estimates background in the source region (src) with the observed count density in the background annulus (back). Using two annuli, the count density in the inner and outer annuli are extrapolated to the center to provide an estimate of the average background in the source region.

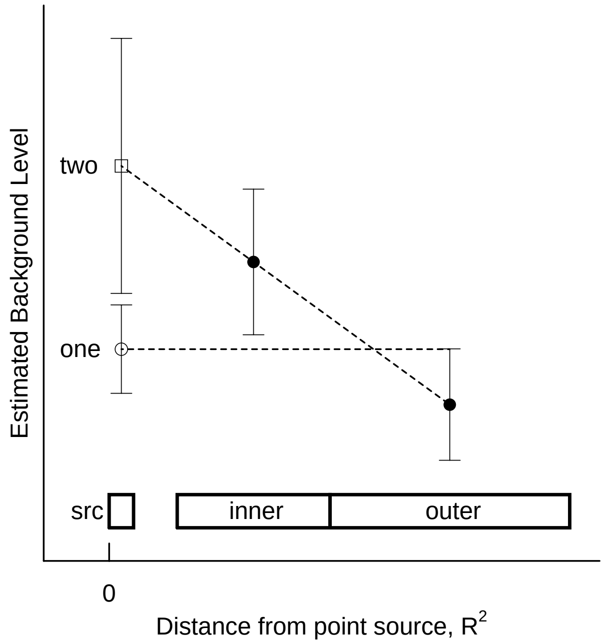

Fig. 3.— The background in the source region (src) is estimated from the counts per pixel in the inner and outer annuli. The two-annulus estimator (open square symbol) provides a direct extrapolation of the outer and inner count densities to the source region. The one-annulus estimator (open circle symbol) treats the inner and outer annuli as a single annulus, and so computes an average of the inner and outer background estimates weighted by their respective areas. The error bars indicate plus and minus one-sigma errors (where "sigma" is the square root of the variance of the estimator) for each of the estimated background levels. The two-annulus estimator has a much larger variance than the one-annulus estimate, but it is unbiased even for cubic polynomial nonuniformities in the background.

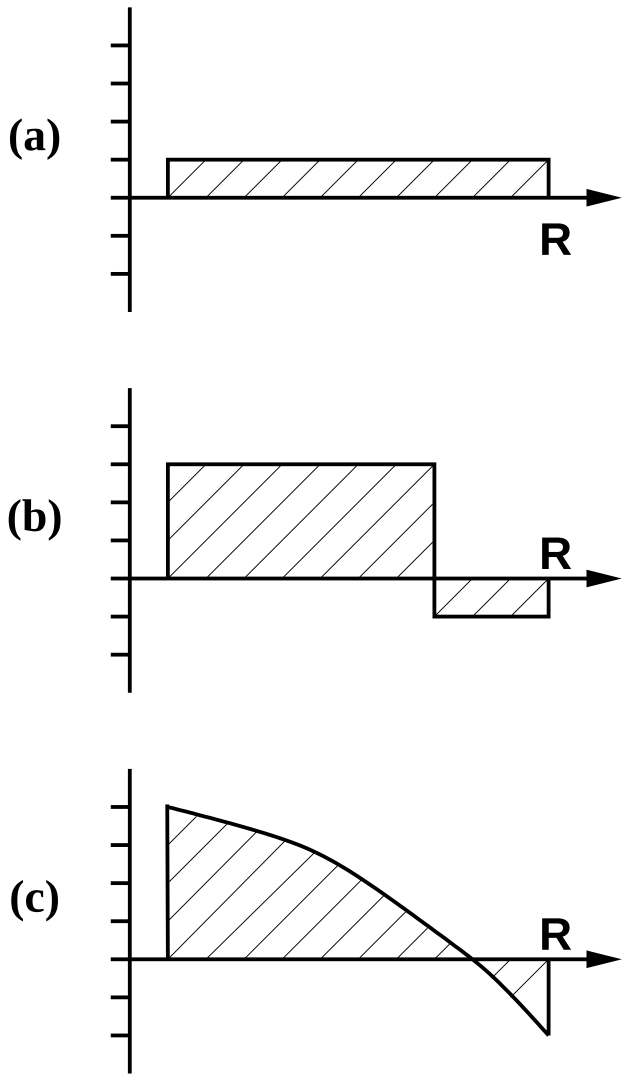

Fig. 4.— Radial kernels for background estimation at the origin: (a) Simple one-annulus estimator; if the background is uniform, then this provides the optimal estimate. (b) Two-annulus estimator; if the background has nonuniformities which can be modelled with a cubic polynomial, then this estimator is unbiased. (c) The continuum limit of a multi-annulus estimator is a kernel function which varies with radius. One can derive an optimal kernel function – see equation (47) – which produces the least estimator variance while being constrained to being unbiased for cubic nonuniformities.

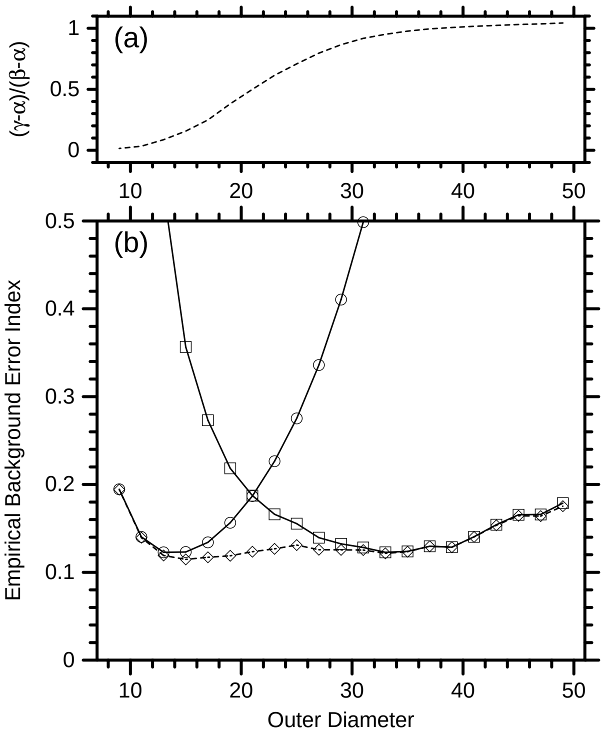

Fig. 5.— The Empirical Background Error Index for the ALEXIS map shown in figure 1a is plotted against outer annulus diameter for the simple one-annulus estimator (circles), for the two-annulus estimator in equation (31) (squares), for the "average best" linear combination of one- and two- annulus estimators (dotted line, with diamonds). A smaller number indicates a more accurate background estimation. The annuli were square with odd-integer diameters; the source region was 3x3 pixels, and the hole was 5x5. For the two annulus estimators, the annulus was partitioned to provide approximately equal areas for the inner and outer annulus. The dotted line in the upper panel shows the coefficient of the best linear combination, rescaled so that a value of zero corresponds to the one-annulus estimator, and a value of one to the two-annulus estimator. For small annuli, the one-annulus estimator is preferred, but for larger annuli, the two-annulus estimator is superior. As the annulus diameter increases further, however, the approximation of the background as a cubic polynomial surface breaks down, and the two-annulus estimator gets worse. At their best annular diameters, the one-annulus and the two-annulus estimators exhibit virtually identical performance for this data set.

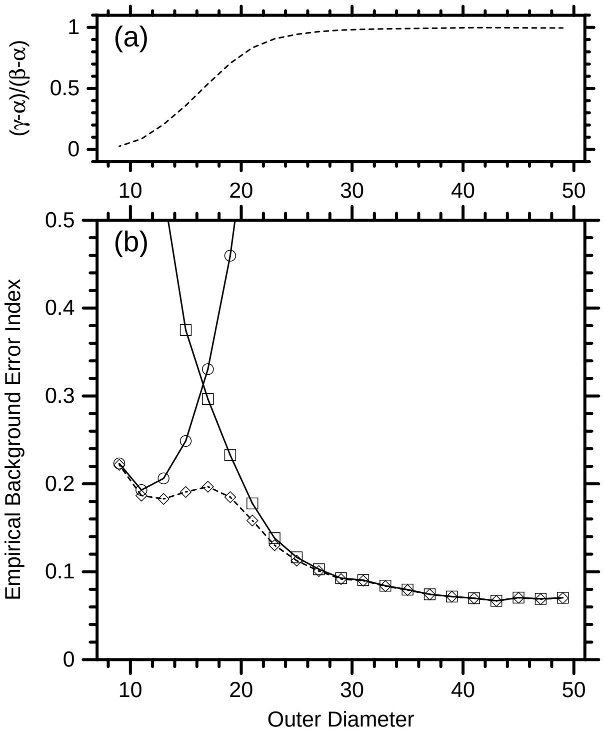

Fig. 6.— The Empirical Background Error Index for the artifical cubic background map shown in figure 1b is plotted in just the same way as shown in figure 5. Again, the one-annulus estimator is preferred if the annulus is small, but the two-annulus estimator is better as the annulus size grows. In this example, since the background is precisely cubic over the entire map, the index decreases essentially monotonically with increasing annulus size.

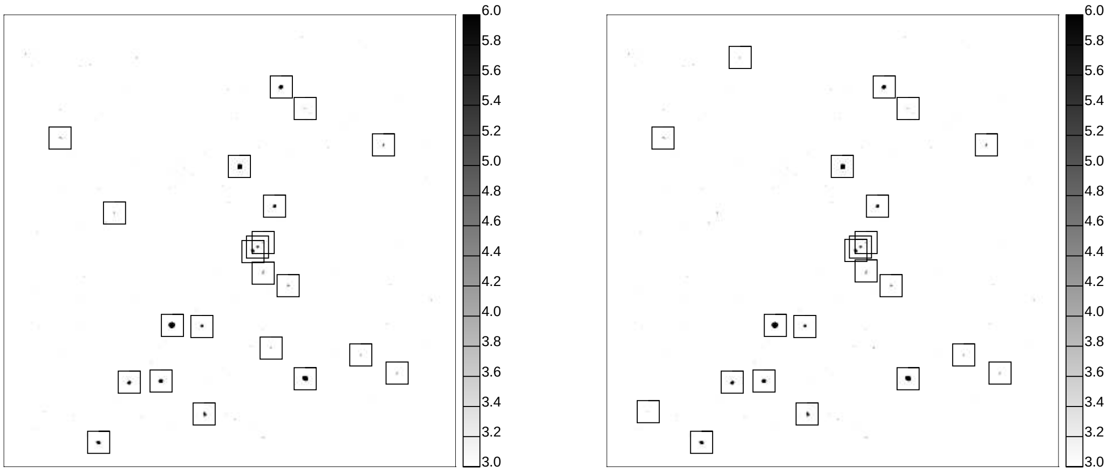

Fig. 7.— Significance map for the ALEXIS map shown in figure 1a, using **(a)** a one-annulus detector with a 13x13 pixel background, and **(b)** a two-annulus detector with a 25x25 inner annulus and a 35x35 outer annulus. In both cases, the source region was 3x3 and the annular hole was 5x5. The significance is in units of "sigmas", or more specifically, the S/N statistic of equation (80). Only significances above three sigmas are shown, and point source detections with $S/N > 4$ are indicated with squares. (Those with $S/N > 5$ are also listed in Table 1.) A number of known white dwarfs and bright O and B starts are visible in this map, including the distinctive belt of Orion, which is near the center of this map.

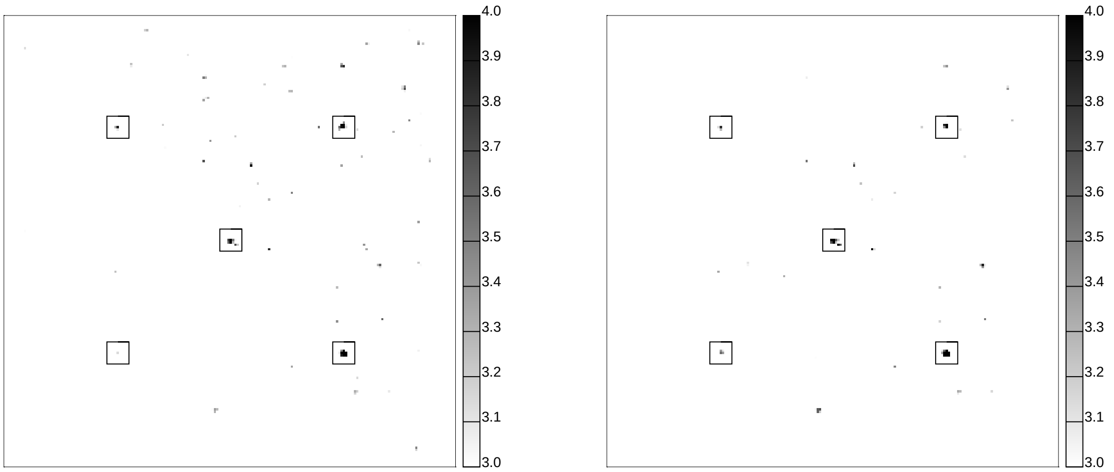

Fig. 8.— Significance map for the artificially generated cubic background map shown in figure 1b, using **(a)** a one-annulus detector with a 13x13 pixel background, and **(b)** a two-annulus detector with a 29x29 inner annulus, and 41x41 outer annulus. In both cases, the source region was 3x3 and the annular hole was 5x5. Point 1 (lower left) is seen to be more significant in the two-annulus map than in the one-annulus map. Also, there is a preponderance of false alarms in the upper right quadrant of the one-annulus map.

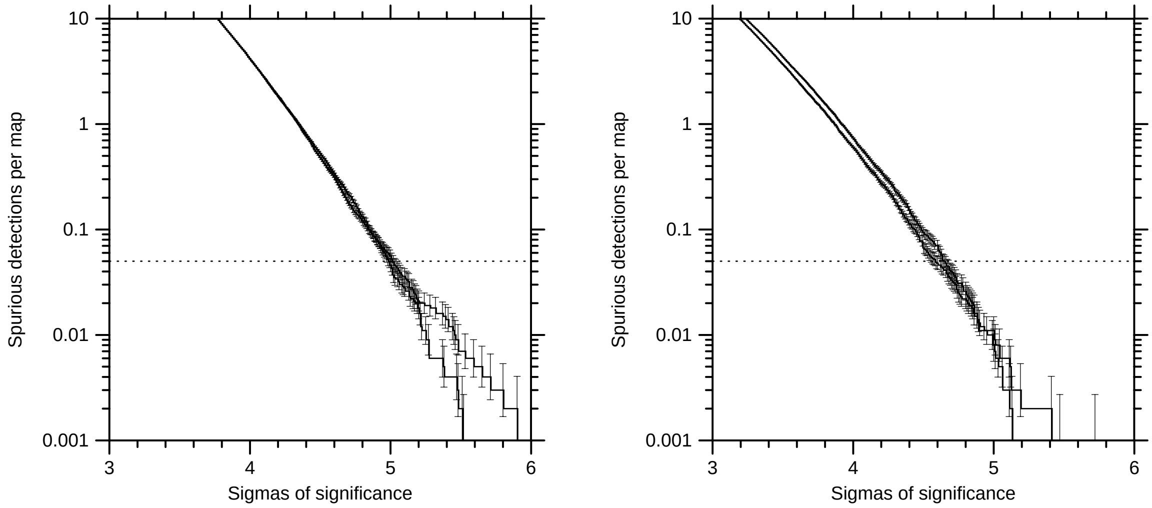

Fig. 9.— Cumulative histograms generated from one thousand surrogate maps of both **(a)** the ALEXIS map (figure 1a) and **(b)** the artificial cubic background map (figure 1b), using both one-annulus and two-annulus point-source detection strategies (annulus sizes are described in the captions to figure 7 and figure 8). The horizontal axis is significance S/N, and the vertical axis is the average number of spurious sources per map which are significant at that level or greater. The dotted line corresponds to the traditional p=0.05 level of significance.

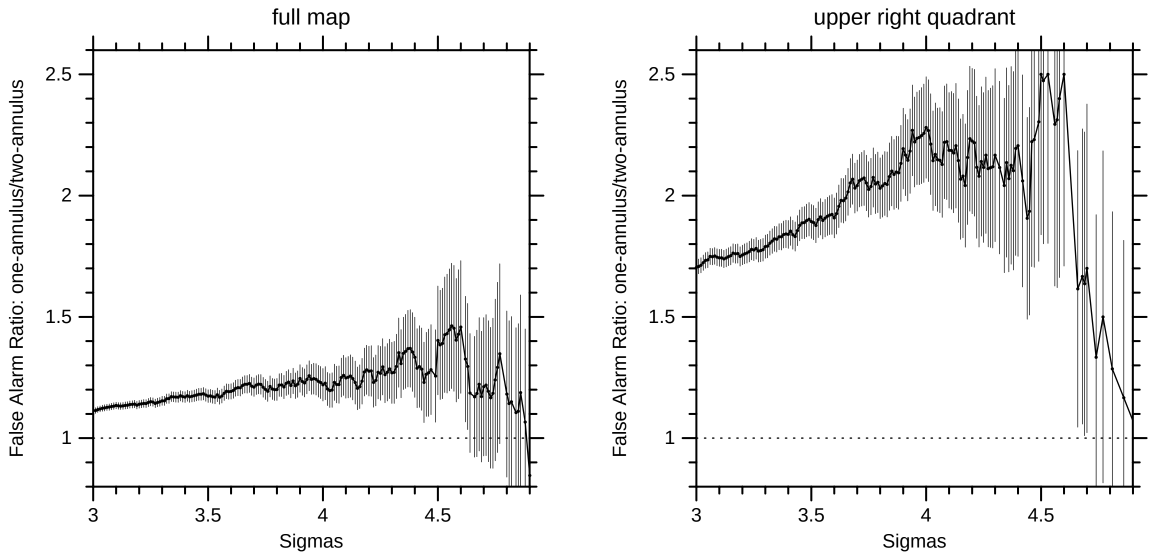

Fig. 10.— **(a)** The ratio of false alarm rates for the one- and two- annulus detectors is shown for the artificial cubic map (see figure 9b). **(b)** We restrict attention to the upper-right quadrant of the cubic map; in this quadrant the background is peak-like, and we see that the false alarm rate is roughly twice as large with the one-annulus detector compared to the two-annulus detector.

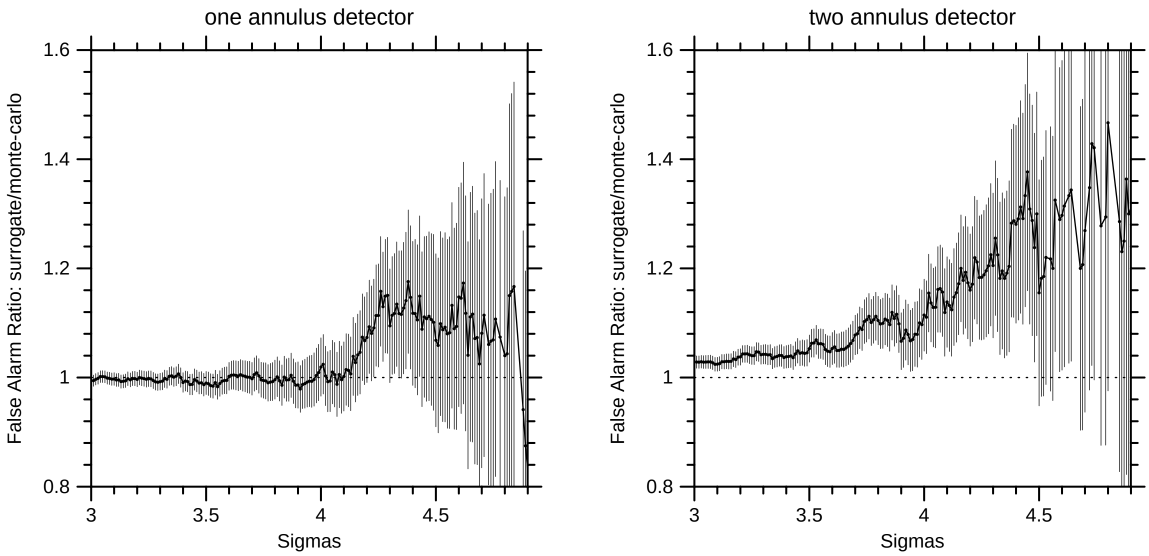

Fig. 11.— The false alarm rate estimated from the surrogate maps is divided by the "true" false alarm rate estimated from a Monte-Carlo run with 1000 realizations of the artificial cubic-background map (with no artificially added point sources). This ratio is plotted against significance threshold for **(a)** the one-annulus detector and **(b)** the two-annulus detector.

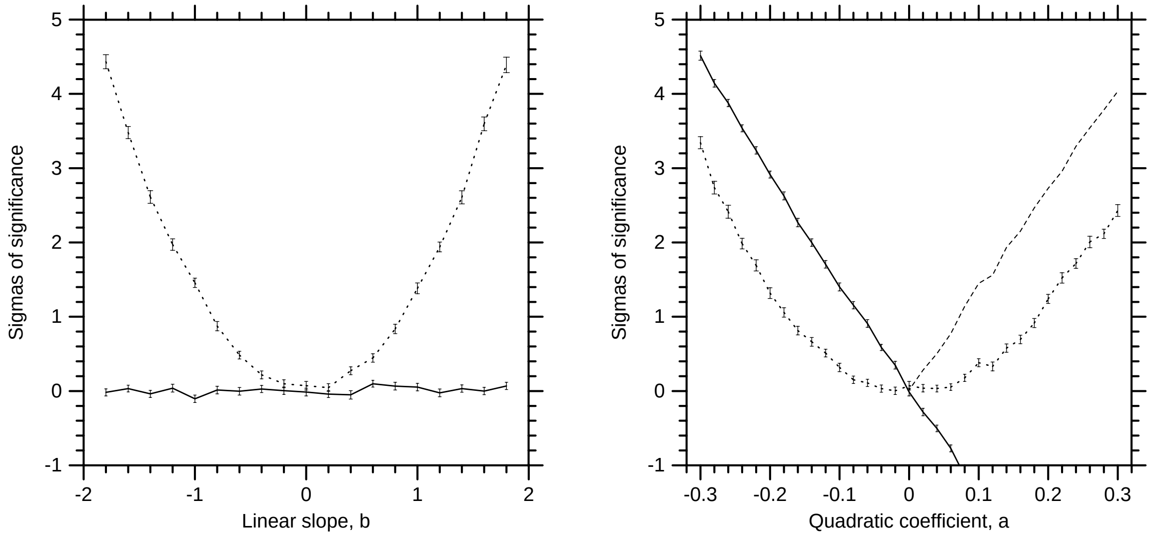

Fig. 12.— Results of a Monte-Carlo experiment comparing the sensitivity of the Poisson Dispersion Index (PDI) (dotted line) in equation (84) with an annulus-based statistic (solid line) in equation (85), over a range of nonuniform backgrounds. The background is generated by a quadratic equation: $B_{ij} = c + bi + a(i^2 + j^2)$, where i, j are the pixel indices with values $i = 0$, $j = 0$ corresponding to the center pixel of a 13x13 map. For each trial, a Poisson realization was constructed for the given background, and the two-annulus statistic (using a 9x9 inner annulus) and the PDI was computed. Both statistics have mean zero and variance one when the background is flat, and so both can be used as a number of sigmas of signficance. Plotted is the mean (with error bars indicating the standard deviation of the mean) value of each statisic for 400 trials. In **(a)**, the slope b is varied while keeping the quadratic coefficient $a = 0$, and in **(b)** the quadratic coefficient a is varied while keeping the slope $b = 0$. In both cases $c = 100$ counts. We see from **(a)** that the annulus-based statistic is completely insensitive to simple linear gradients, whereas the PDI is sensitive even to gradients of order one percent per pixel. (We do not mean to advocate the PDI as a sensitive detector of gradients; the high sensitivity in this case is a function of the relatively large counts per pixel and the large number of pixels in the background annulus.) By contrast, we see from **(b)** that the annulus-based statistic is more sensitive to small quadratic nonuniformities. Note that a negative coefficient a corresponds to a "peak" in nonuniformity, and these peaks in the background are just the artifact that are most likely to lead to spurious source detections. Positive values of a ("valleys" in the background) lead to negative significance. If a two-tailed test of flatness is desired, then the absolute value of the statistic should be used; this is shown as a dashed line in this plot.

Table 1. Point source detections in the ALEXIS map with S/N>5

ID	Coordinates RA	Dec	Significance S/N Two-annulus	One-annulus
Sirius B	101.11	−16.84	38.63	37.65
RE J0457−280	74.24	−28.25	24.26	23.75
WD 0549+158	88.09	15.96	17.16	16.17
RE J0515+324	78.74	32.72	10.17	10.14
ϵ CMa[a]	104.45	−29.05	9.53	8.74
ζ Pup[a]	120.68	−39.96	9.17	9.34
RE J0723−274	110.73	−27.80	8.52	8.55
ζ Ori[a]	85.13	−1.83	8.30	7.69
γ Ori[a]	81.20	6.42	7.25	7.05
RE 0623−374	95.85	−37.65	6.20	6.55
β CMa[a]	95.51	−18.14	6.15	5.88
ϵ Ori[a]	84.08	−1.19	6.13	5.52
β Ori[a]	78.47	−8.30	5.51	5.08
V471 Tau	57.39	17.39	5.11	5.12

[a]These sources are bright O and B stars, and are likely to have been detected because of known UV leaks in the detector filters, not because of radiation in the ALEXIS bandpass.

Table 2. Significance of artificial points in cubic background map

Point	Significance S/N[ac] Two-annulus	One-annulus	Background nonuniformity[bc] Large Annuli	Small Annuli
1	3.55	3.11	−49.67	−1.50
2	3.82	3.77	0.01	−0.06
3	3.98	4.20	20.68	0.54
4	3.83	3.77	0.02	−0.00
5	3.84	3.70	0.03	0.08

[a]If the background were known exactly, the nominal significance for these artificial points would be $S/N = 4.0$.

[b]This statistic is defined in Section 4.4. The large annuli are 29×29 and 41×41; the small annuli are 9×9 and 13×13.

[c]The statistical error for all the numbers reported in this table is ±0.03.